J. Astrophys. Astr. (2006) **27,** 167–173

Flare Ribbon Expansion and Energy Release

Ayumi Asai[1,*], Takaaki Yokoyama[2], Masumi Shimojo[1],
Satoshi Masuda[3] & Kazunari Shibata[4]
[1]*Nobeyama Solar Radio Observatory, Minamisaku, Nagano, 384-1305, Japan.*
[2]*Department of Earth and Planetary Science, University of Tokyo, Hongo, Bunkyo, Tokyo, 113-0033, Japan.*
[3]*Solar-Terrestrial Environment Laboratory, Nagoya University, Toyokawa, Aichi 442-8507, Japan.*
[4]*Kwasan and Hida Observatories, Kyoto University, Yamashina, Kyoto 607-8471, Japan.*
[*]*e-mail: asai@nro.nao.ac.jp*

Abstract. We report a detailed examination about the relationship between the evolution of the Hα flare ribbons and the released magnetic energy during the April 10 2001 flare. In the Hα images, several bright kernels are observed in the flare ribbons. We identified the conjugated footpoints, by analyzing the lightcurves at each Hα kernels, and showed their connectivities during the flare. Then, based on the magnetic reconnection model, we calculated quantitatively the released energy by using the photospheric magnetic field strengths and separation speeds of the Hα flare ribbons. Finally, we examined the downward motions which are observed at the Hα kernels. We found that the stronger the red-asymmetry tends to be associated with the brighter the Hα kernel.

Key words. Sun: activity—Sun: flares, chromosphere, corona, X-rays, gamma rays.

1. Introduction

Based on the CSHKP magnetic reconnection model (Carmichael 1964; Sturrock 1966; Hirayama 1974; Kopp & Pneuman 1976), we can explain several well-known features associated with solar flares (see Fig. 1). The Hα flare ribbons, for example, are caused by the precipitation of nonthermal particles and/or the effect of thermal conduction which are produced after magnetic field lines reconnect in the corona. At successive reconnections, the reconnection points (X-points) move upward, and therefore, newly reconnected field lines have their footpoints further out than the footpoints of the field lines that have already reconnected, which leads us to recognize the 'apparent' separation motion of the flare ribbons. The Hα flare ribbons are located on either side of the magnetic neutral line, and have magnetic polarities opposite to each other. The evolution of the flare ribbons, therefore, has some information on the energy release mechanism.

In this paper we report a detailed examination of the flare ribbon evolution during an X2.3 solar flare which occurred on April 10, 2001. We examined fine structures inside

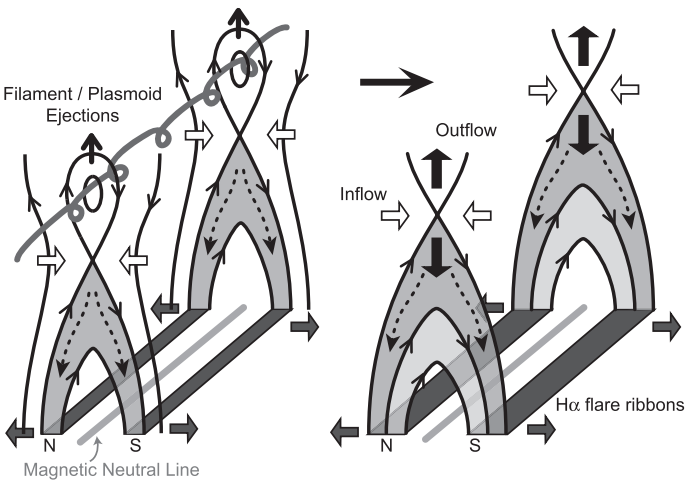

Figure 1. Cartoon of magnetic reconnection. Solid lines show the magnetic field lines. N and S show the magnetic polarities. Reconnected magnetic field lines form post-flare loops with a cusp shaped structure (gray regions). Along the reconnected loops, nonthermal particles and thermal conduction propagate from the reconnection site to the footpoints (dashed arrows). As they precipitate into the chromosphere the Hα flare ribbons are generated at the footpoints (dark gray region). They are located on either side of the magnetic neutral line (light gray line), and have magnetic polarities opposite to each other.

flare ribbons by using the Hα images. We identified the conjugate footpoints of each Hα kernel by using cross-correlation functions of the light curves, and examined their temporal evolution. Next, we estimated the amount of the released magnetic energy quantitatively by using the separation speed of the flare ribbons and the photospheric magnetic field strength. Then, we examined the downward motions observed at the Hα kernels. The precipitation pushes the chromospheric plasma downward and modulates Hα emission line at the footpoints of the reconnected loops, which is observed as red-shifted emission line, called a "red-asymmetry". We investigated when and where strong red-asymmetry features.

2. Observations

We observed a typical two-ribbon flare (X2.3 on the GOES scale) which occurred in the NOAA Active Region 9415 (S22°, W01°) at 05:10 UT, April 10, 2001 with the 18 cm Sartorius Refractor (*Sartorius*) at Kwasan Observatory, Kyoto University. The Hα monochromatic images of the flare were obtained with the temporal and spatial resolution of about 1 s and 1″, respectively. During the observation, the exposure time was properly regulated so that the fine structure inside the flare ribbons, like Hα kernels, can be clearly seen without saturating. The flare was also observed with 60 cm Domeless Solar Telescope (DST) at Hida Observatory, Kyoto University. Hα $\pm$ 0.0 Å, +1.5 Å, and −1.5 Å images were taken with the temporal and the spatial resolutions of about 30 s and about 0.6″, respectively. The extreme-ultraviolet (EUV) images of the flare were obtained with *Transition Region and Coronal Explorer* (*TRACE*; Handy *et al.* 1999; Schrijver *et al.* 1999). *TRACE* 171 Å images clearly show post-flare loops which

confine $\sim$ 1 MK-plasma. The flare ribbons in the *TRACE* 171 Å images nearly simultaneously appear with the Hα flare ribbons, while the formation of the post-flare loops are noted after the evolution of the flare ribbons. This is because it takes a certain time for hot plasma, which is heated up to about 10 MK or more, to cool down to 1 MK.

To examine the locations of the HXR radiation sources where strong energy releases occur, and to compare the temporal variations of the estimated energy release rates with the light curve of the HXR total intensity, we used HXR data taken with the hard X-ray telescope (HXT; Kosugi *et al.* 1991) aboard *Yohkoh* (Ogawara *et al.* 1991). The temporal resolution of the HXT data is 0.5 s. We also used microwave time profiles obtained with the Nobeyama Radioheliograph (NoRH; Nakajima *et al.* 1994). The NoRH microwave data were obtained at 17 GHz with a temporal resolution of 1.0 s. Both the HXT and NoRH light curves show some bursts. The dawn of *Yohkoh* was at 00:19 UT, and the earlier part of the flare was missed because of night. No large NoRH bursts are seen from 00:20 to 00:31 UT, since the emission mechanism becomes optically-thick during the time range, while the other bursts are from optically-thin gyrosynchrotron radiation. Photospheric magnetograms were taken with the Michelson Doppler Imager (MDI; Scherrer *et al.* 1995) onboard the *Solar and Heliospheric Observatory* (SOHO; Domingo *et al.* 1995). We co-aligned the Hα images and the MDI images visually. The accuracy of the co-alignment is about 2″, which is comparable to the pixel size of the MDI data.

3. Identification of conjugate footpoints

Firstly, we identified the conjugate pairs of the footpoints seen in the Hα images by a new method which Asai *et al.* (2003) suggested. Figure 2(a) and (b) show a photospheric magnetogram taken with the MDI and an Hα image obtained with *Sartorius*, respectively. We divided the Hα flare ribbons, which have the magnetic polarities opposite to each other, into fine meshes (see Fig. 2c). Then, we drew light curves of total intensity for each box in both the meshes, and identified the highly-correlated pairs (conjugated pairs) by calculating the cross-correlation functions. In Fig. 2(c) *black solid* lines are drawn to connect such highly-correlated pairs.

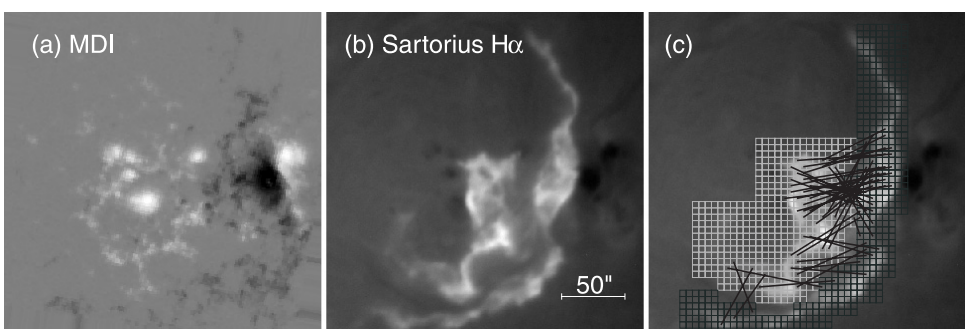

Figure 2. Method of analyses. Celestial north is up, and west is to the right. **(a)** Photospheric magnetogram taken with *SOHO* MDI. **(b)** Raw Hα image of the *Sartorius* at 05:31 UT. **(c)** Hα image overlaid with the fine meshes and with black solid lines which connect highly-correlated pairs on (b). The left (east) mesh lines is positive polarity (drawn with light gray lines), and the right (west) one (dark gray lines) is negative polarity.

Then, we examined the spatial relationship between the post-flare loops seen in the EUV images and the conjugated pairs of the Hα kernels. We checked whether the Hα pairs are actually connected by the 171 Å flare loops or not, and found that almost all the pairs are connected by the flare loops. This good coincidence between the Hα pairs and the flare loops strongly supports the scenario of the flare loop formation: the EUV flare loops are formed by the plasma evaporated from the brightening Hα pairs. We also examined, in detail, the temporal and spatial evolution of the pairs of the Hα conjugate footpoints selected above. The start times of brightening of each Hα pair tell us the site and the time of the energy release or the magnetic field reconnection. Thus, we follow the evolution of the energy release sites by examining the fine structures inside the flare ribbons or Hα kernels. At the beginning, the Hα kernels and the conjugated pairs appear nearly parallel to the magnetic neutral line or are in a strongly sheared configuration. As the flare progresses, the flare ribbons quickly separate from each other, and many Hα kernels appear successively. The locations of the Hα kernels tend to move toward northeast in the eastern ribbon and southwest in the western ribbon. Such changes from the strongly-sheared to less-sheared directions of the lines that are connecting Hα pairs indicate the configuration of the height-dependent sheared magnetic field in the corona over the neutral line.

4. Energy release rate

Secondly, we estimated the amount of energy released via magnetic reconnection during the flare (see Asai *et al.* (2004) for more details). Based on the reconnection models, the energy release rate can be written as the product of the Poynting flux into the reconnection region S $(= 2(4\pi)^{-1}B_c^2 v_i)$ and the area of the reconnection region A as follows:

$$\frac{dE}{dt} = SA = 2\frac{B_c^2}{4\pi} v_i A, \tag{1}$$

where B_c is the magnetic field strength in the corona and v_i is the inflow velocity into the reconnection region. Note that this assumption is based on the 2D expression of the magnetic reconnection model. It is very difficult to measure the coronal magnetic field strength B_c and the inflow velocity v_i directly. Consequently, an indirect method is needed to evaluate the energy release rate quantitatively by using observable values. We assume that the area of the reconnection region A does not change significantly during the flare and is independent of the magnetic field strength, and that the energy release rate is simply proportional to the Poynting flux S.

Here, we examined the relation between the expanding motions of the Hα flare ribbons and the released magnetic energy by using the magnetic field strengths at the photospheric level B_p and the separation speed of the flare ribbons v_f, instead of direct coronal values such as B_c and v_i. We estimated the reconnection rate $\dot{\Phi}$, i.e., the electric field strength in the corona. The reconnection rate is one of the most important physical values in reconnection physics, because it shows how violently magnetic reconnection progresses. It is defined as the reconnected magnetic flux per unit time, and expressed as $\dot{\Phi} = B_c v_i$. From the conservation of magnetic flux, we can write $\dot{\Phi} = B_p v_f$. We also estimated the Poynting flux S. If we assume that the area of the reconnection region (A) does not change significantly during the flare and is independent of the

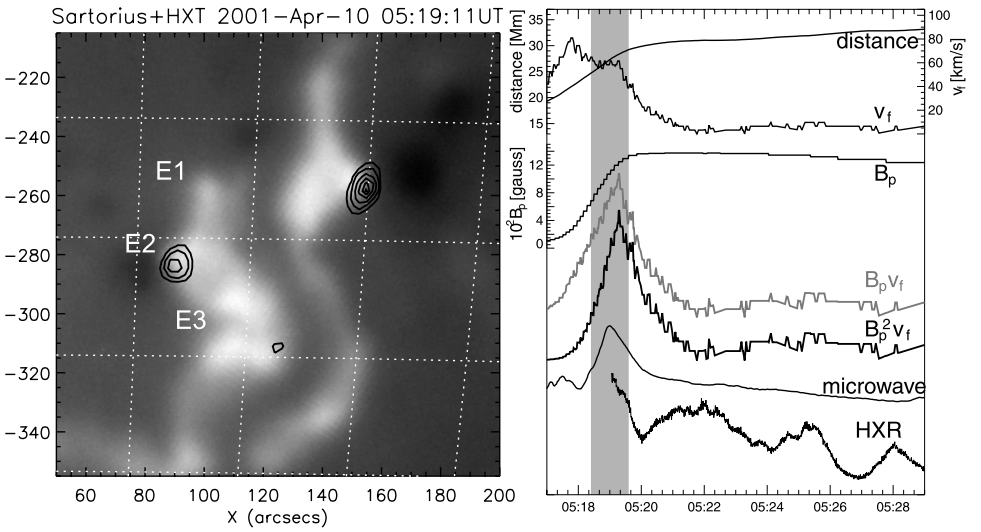

Figure 3. **Left:** Hα image kernels overlaid with HXR contour image. E1, E2, and E3 show Hα kernels. Only E2 is associated with the HXR emission source. **Right:** Temporal variations of the physical parameters measured along the slit line which passes through the E2 Hα kernel. **From top to bottom:** distance of the outer edge of the ribbon from the magnetic neutral line; separation speed of the ribbon (v_f); photospheric magnetic field strength (B_p) at the outer edge of the ribbon; estimated reconnection rate $\dot{\Phi}$ (gray lines); estimated Poynting flux S; microwave correlation plot in 17 GHz obtained with NoRH; HXR count rate measured in the Yohkoh/HXT H band (53–93 keV).

magnetic field strength, the S is written as $2(4\pi)^{-1}B_c^2 v_i$. Furthermore, it is rewritten as $S \propto B_p^2 v_f$ with the assumption that B_c is proportional to B_p in the same ratio all over the flaring region. Although the assumption may be simplistic, it is reasonable, provided we do not discuss the energy release rates of the whole active region. This is because the B_c-to-B_p ratio remains approximately constant in narrow regions.

In the April 10, 2001 flare, the expansion motion of the flare ribbons is roughly seen in the east–west direction, since the magnetic neutral line lies approximately in the celestial north–south direction (see Fig. 2b). Therefore, we put slit lines in the east–west direction so that each passes the flare ribbons perpendicularly, and tracks the positions of the outer edges of the ribbons along the slit lines. In the right panel of Fig. 3, we show the temporal variation of the physical parameters, such as B_p, v_f, $\dot{\Phi}$, and S along a slit line. Here, we defined v_f as the speed of the flare-ribbon separation, relative to the magnetic neutral line, in the perpendicular direction. The right panel of Fig. 3 also shows the estimated $\dot{\Phi}$ and S compared with the light curves in HXR and microwaves which were obtained with HXT and NoRH. The evolutions of the reconnection rates and Poynting fluxes appear to match the HXR and microwave light curves well (see vertical light gray lines).

Are the estimated energy release rates at the Hα kernels associated with the HXR bursts large enough to explain the difference between the spatial distribution of the HXR sources and that of the Hα kernels? To answer the question, we compared them with those at the Hα kernels without HXR bursts, e.g., E1 and E3 in the left panel of Fig. 3, at the time of the first HXR burst (05:19UT). We found that the reconnection

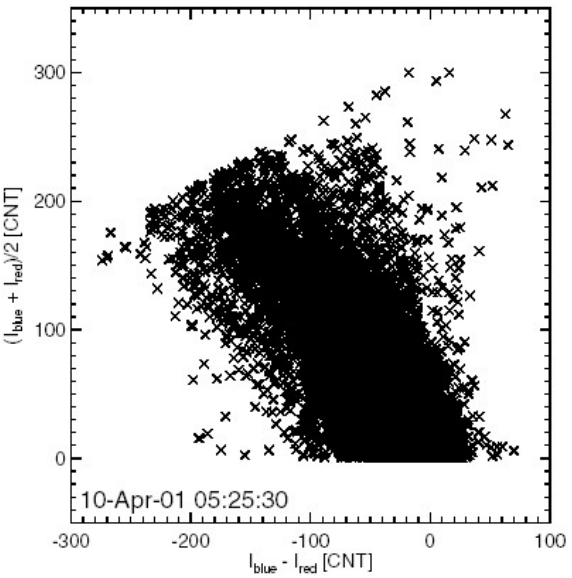

Figure 4. Scatter plot between the red-asymmetries and the intensities of the Hα kernels. The horizontal axis shows the differential between $I_{\rm blue}$ and $I_{\rm red}$. The vertical axis shows their averaged intensity.

rate of E2 is at least 16 times stronger than that of the other two kernels. The Poynting flux at E2 is also much more enhanced, and is 150 times stronger than that of the others. Both the estimated reconnection rates and Poynting fluxes are large enough locally at the HXR sources. The results can explain the difference between the spatial distribution of the HXR sources and that of the Hα kernels.

5. Red asymmetry

Finally, we examined the evolution of the Hα kernels spectroscopically. At Hα kernels, the precipitation of the nonthermal particles and/or thermal conduction into the chromosphere generate the downward compression of the chromospheric plasma, which is observed as the reddening of Hα emission (Ichimoto & Kurokawa 1984). The authors also reported that the red-shift corresponds to the downward motion with a speed of about 50–100 km s^{-1}, based on their spectroscopic observations.

We measured the differential between the Hα intensity in the red-wing (H$\alpha + 1.5$ Å) and that in the blue-wing (H$\alpha - 1.5$ Å), that is, how bright are the red-wing images by using the Hα wing data obtained with DST, and examined the spatial distribution of the red-asymmetry. We found that the red-asymmetry appears all over the flare ribbons during the impulsive phase of the flare, and above all it is conspicuous at the outer edges of the flare ribbons. We also examined the relationship between the red-asymmetry and the intensity of the Hα kernels. Figure 4 shows the scatter plot between the red-asymmetry ($I_{\rm blue} - I_{\rm red}$; horizontal axis) and the averaged Hα intensity ($(I_{\rm blue} + I_{\rm red})/2$; vertical axis) at the kernels. We can see the tendency that the stronger red-asymmetry (brighter in the red-wing images) is associated with the brighter Hα kernel.

6. Summary and discussions

We examined in detail the fine structure and the temporal and spatial evolution of the Hα flare ribbons associated with the April 10, 2001 flare.

We identified the conjugate footpoints in both the flare ribbons by calculating cross-correlation functions, and confirmed that the pairs of Hα conjugate footpoints are really connected by the post-flare loops seen in the EUV images. This result strongly supports the flare scenario that the Hα kernels are brightened by the precipitation of high energy electrons or by heat conduction and that evaporated plasma from the Hα kernels produce the high-temperature flare loops observed in SXR and EUV. Our finding suggests that we can study the magnetic field configuration in the energy release sites by examining evolution of Hα kernels. We have been able to follow the formation of the flare loops and the evolution of energy release sites. Next, we estimated the energy release rate quantitatively, based on the magnetic reconnection model, by using the photospheric magnetic field strength and the separation speed of the Hα flare ribbons. The estimated energy release rates of the Hα kernels associated with the HXR sources are locally large enough to explain the difference between the spatial distribution of the Hα kernels and the HXR sources. The temporal evolution of the energy release rates also shows peaks corresponding to the HXR bursts. Then, we examined spatially resolved red-asymmetry distributions and their temporal evolution, by using Hα wing images. Red-asymmetry tells us the quantitative information of the precipitation (nonthermal particles/thermal conduction). We found the tendency that the stronger red-asymmetry is associated with the brighter Hα kernel.

Acknowledgements

We made extensive use of the TRACE Data Center, Yohkoh Data Center and SOHO MDI Data Service.

References

Asai, A., Ishii, T. T., Kurokawa, H., Yokoyama, T., Shimojo, M. 2003, *Astrophys. J.*, **586**, 624.
Asai, A., Yokoyama, T., Shimojo, M., Masuda, S., Kurokawa, H., Shibata, K. 2004, *Astrophys. J.*, **611**, 557.
Carmichael, H. 1964, In: *The Physics of Solar Flares* (ed.) Hess, W. N., (NASA SP-50), p. 450.
Domingo, V., Fleck, B., Poland, A. I. 1995, *Solar Phys.*, **162**, 1.
Handy, B. N. *et al.* 1999, *Solar Phys.*, **187**, 229.
Hirayama, T. 1974, *Solar Phys.*, **34**, 323.
Ichimoto, K., Kurokawa, H. 1984, *Solar Phys.*, **93**, 105.
Kopp, R. A., Pneuman, G. W. 1976, *Solar Phys.*, **50**, 85.
Kosugi, T. *et al.* 1991, *Solar Phys.*, **136**, 17.
Nakajima, H. *et al.* 1994, *Proc. IEEE*, **82**, 705.
Ogawara, Y., Takano, T., Kato, T., Kosugi, T., Tsuneta, S., Watanabe, T., Kondo, I., Uchida, U. 1991, *Solar Phys.*, **136**, 1.
Scherrer, P. H. *et al.* 1995, *Solar Phys.*, **162**, 129.
Schrijver, C. J. *et al.* 1999, *Solar Phys.*, **187**, 261.
Sturrock, P. A. 1966, *Nature*, **211**, 695.